Assiut Univ. J. of Geology
45(1), p-p35- 65(2016)

MONITORING AND MANAGEMENT OF WATER LOGGING PHONOMENA USING GEOELECTRICAL AND HYDROLOGICAL TECHNIQUES IN EL BUSTAN AREA, WESTERN PART OF THE DELTA

***Al Temamy, A. M.M. and *Ibrahim, S. M.M.**

**Desert Research Center (DRC), I Mathaf El-Mataryia Street, El-Mataryia, Cairo, Egypt.*

Received: 13/2/2015 **Accepted:** 28/1/2016

The desert lands lying to the west of the Nile Delta represent the natural extension areas of the Nile Delta where the old agricultural reclamation projects are started since 1950s. El-Bustan area represents one of these areas where the reclamation process started in the last decade of the 20th century. The continuous rising of the groundwater level caused the problem of water logging and deterioration of the reclaimed lands in the area. The integrated geoelectrical and hydrological studies through the present study will help in the solution of such problems through the monitor of the groundwater parameters (depth to water, water levels and salinity) with time. The quantitative interpretation of the geoelectrical measurements and the hydrological data of the drilled wells in 1992 and the present work led to the detection of three main geoelectrical units (A, B, and C). Unit "A" consists of dry clayey sand, sand and gravels sometimes intercalated with clay lenses. The thickness of this unit represents the depth to water which ranging between 9 - 28 m in 1992 and 2 – 23 m in 2011 . The decrease in the thickness of this unit in 2011 was reflecting an increase of the water level with time through vertical percolations of irrigated water or lateral seepage from the surface canals that causing the problem of water logging. Unit "B" represents the water-bearing formation in the study area, the upper part of this unit consists of clayey sand and sand deposits changing at the lower part to clayey sand, gravely sand and gravels having higher resistivity than that of the upper part. Unit "C" represents the last detected geoelectrical layer exhibiting relatively low resistivity values compared with that of the upper two units reflecting an increase in clay content. The interpretation of the 2-Dimension electrical resistivity tomography (ERT) profiles that carried out perpendicular to El-Bustan Canal revealed the presence of seepage from El-Bustan canal to the aquifer. The water level varies from 3 to 15m in 1992 and from 8 to 25m in 2011 with general increase with time which considered as one of the main reasons that causing the problem of the water logging. The water salinity varies from 662 to 1571ppm in 1992 and from 505 to 1507ppm in 2011 with general decrease with time reflecting the seepage of the fresh surface water of El-Bustan Canal to the aquifer. The integration of the geoelectrical and hydrological studies led to define precisely the causes of the water logging problem in the area. Through the periodical monitor and good management of the groundwater parameters as well as constructing good drainage systems will solve the effect of the water logging problems and

consequently decrease the deterioration of the reclaimed areas which finally will disappear and leading to increase the land productivity of such areas.

***Keywords*:** Groundwater, water logging, geoelectrical, hydrological, monitor, management.

INTRODUCTION

The desert lands lying to the west of the Nile delta represent the natural extension areas of the Nile delta. Therefore, economically, the reclamation and development of such areas will have low costs comparable with the other desert districts of Egypt as being near from the urban areas. Regionally, since 1950s intensive development in the land reclamation (About 110000 Hectar), using both surface water and groundwater resources were attracted the attention of the governorate. The old agricultural reclamation projects using surface water are located in the areas adjacent to El-Nasr and El-Nubariya Canals as well as El-Rayah El-Naseri. While, the new projects (About 42000 Hectar) are located in El-Bustan Extension Canal area. El Bustan area represents one of these areas where the reclamation process started early in the last decade of the 20^{th} century. The continuous rising of the groundwater level in such area caused water logging and deterioration of the reclaimed lands. To find solutions for these problems, an integrated geoelectrical and hydrological studies were carried out to monitor rise in groundwater level and deterioration in water quality with time to assist in proposing groundwater management program.

Drawing attention to the existing problem represented in the rise of the groundwater table with time and controlling this phenomenon to promote sustainable development in the investigated area are the main objectives of this study. To find solutions for these problems, an integrated geoelectrical and hydrological studies were carried out to monitor rise in groundwater level and deterioration in water quality with time to assist in proposing groundwater management program.

The study area lies about 17 km east of km 143 (Cairo-Alexandria Desert Highway) representing one of the newly reclaimed areas through the last decade which suffering from the problem of water logging. The area of study lies between latitudes 30° 38` & $30^{\circ}$ 42` N and longitudes 30° 17` & $30^{\circ}$ 20` 10`` E (Fig.1). It is characterized by long hot summer and short warm winter. The mean annual rainfall is about 40.4mm, the mean relative humidity is 65.4% and the average evaporation rate is about 7.7mm/d.

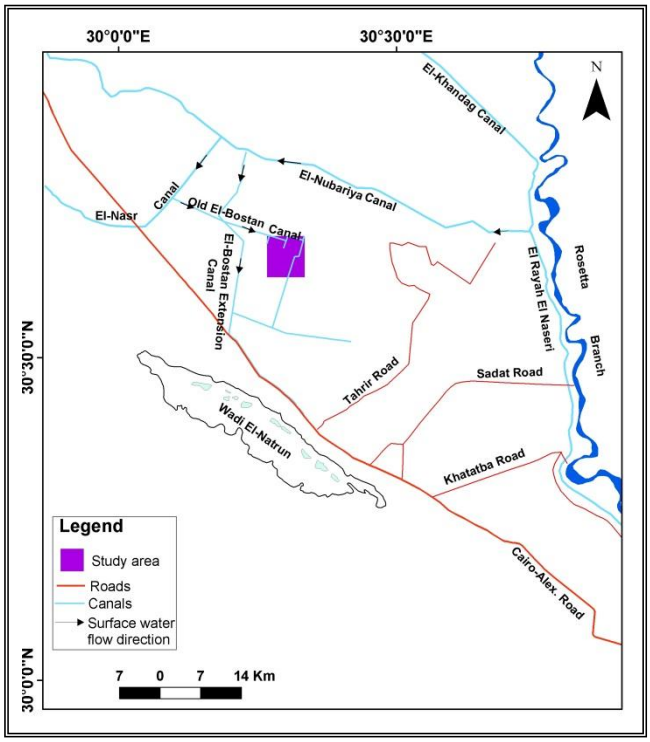

Fig. 1: Location of the study area

GEOMORPHOLOGY, GEOLOGY AND HYDROGEOLOGY

Geomorphologically, the area west of the Nile Delta constitutes a portion of the great arid belt covering Egypt dividing into four geomorphic units (Shata and El Fayoumy) [1] namely; the alluvial plains, the structural plains, the tablelands and the drifting sand. The alluvial plains are differentiated into two main units namely; Young alluvial plains (Recent flood plains) and old alluvial plains (gravelly terraces). The investigated area is a part of the old alluvial plain.

Since the topography and the slope of the study area are necessary in the monitoring of the water logged areas, so the Digital Elevation Model from SRTM data acquired by the National Aeronautics and Space Administration (NASA) and National Imagery and Mapping Agency (NIMA) in February 2000 aboard of the spaceship Endeavour was used (Fig. 2).

Geologically, the study area is covered by sedimentary rocks belonging to the Quaternary. It is dominated by aeolian sand stretching all over the area

in the form of sand sheets (Fig. 3). These deposits are underlain by lagoonal deposits that composed of gypsiferous sticky dark clay and sand. The lagoonal deposits overlie deltaic deposits consisting of medium quartz sand with variable amounts of gravels and clays. The base of the deltaic deposits is defined by Lower Pliocene pyretic clay or sandy clay overlie the Pliocene

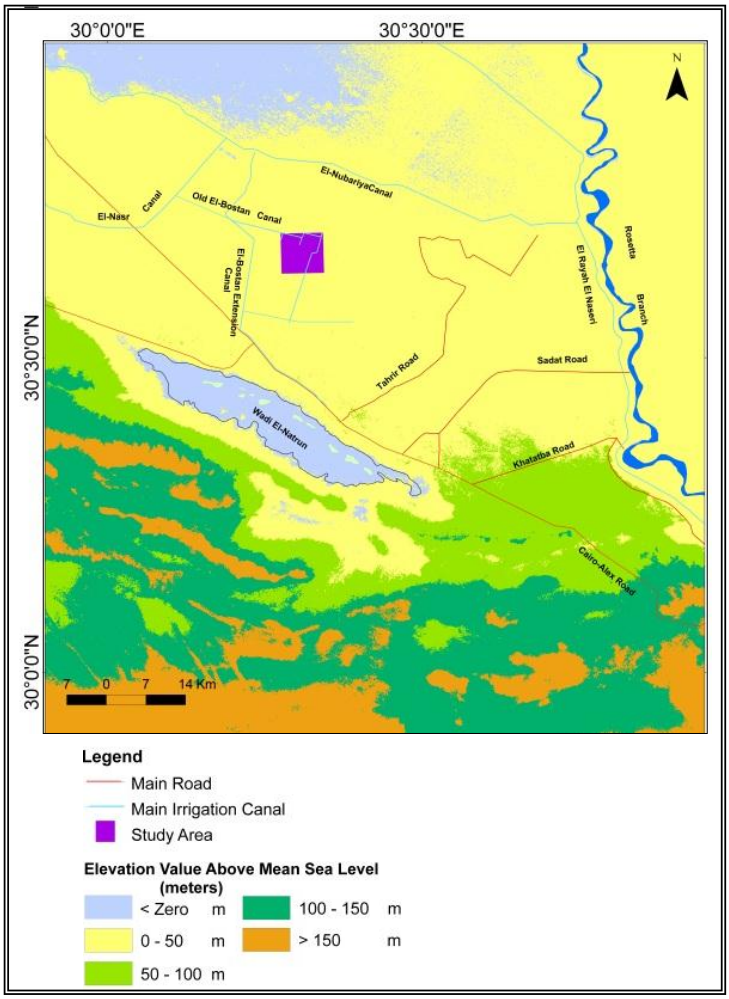

rocks (Tertiary) which are dominated by green clay (Shata et.al) [2].

Fig. 2: Digital Elevation Model (DEM) of the West Nile Delta

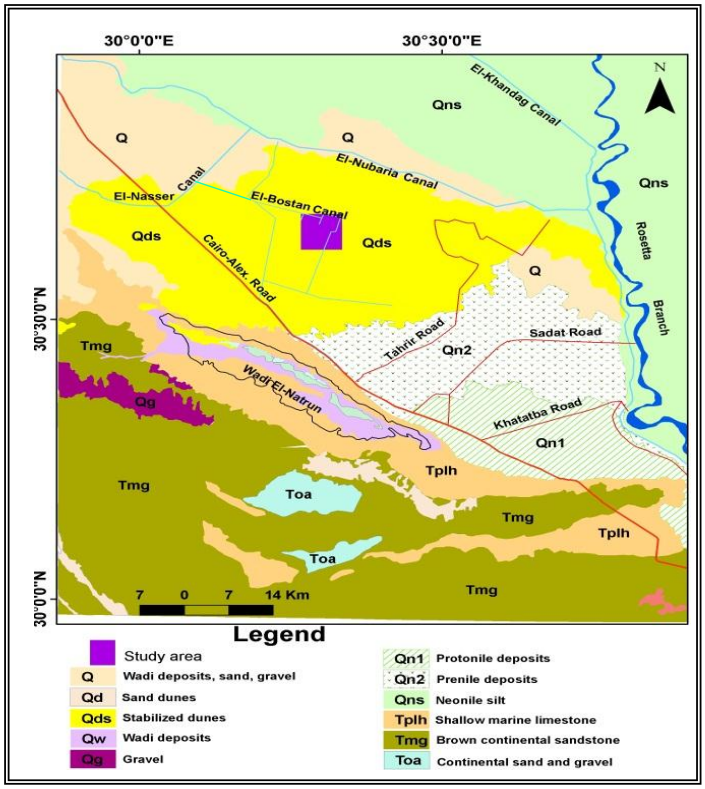

Fig. 3: Geologic map of the West Nile Delta (After CONOCO) [3].

Hydrogeologically, the water resources in the study area are the groundwater and surface water systems. The water-bearing formations in the area west of the Nile delta comprise four aquifers; Recent, Pleistocene, Pliocene and Miocene. Emphasis will be given to the Pleistocene aquifer as it represents the main water-bearing formation in the area of study. The Pleistocene aquifer is composed of successive layers of sand and gravel with some clay lenses. The thickness of this aquifer varies from 60 to 80m near Wadi El Natrun and increases progressively eastwards. The Pleistocene aquifer is directly recharged from the main groundwater basin underlying the Nile Delta, the surface seepage from the cultivated lands as well as from the main irrigation canals. The groundwater of the Pleistocene aquifer varies in quality from fresh to brackish (Abdel Baki) [4]. and (Ibrahim) [5]..

The water bearing formation in El Bustan area comprises two layers, where the clay content is higher in the upper layer comparable with the lower one. On the other hand, the clay lenses overlying and

underlying the water table have negative effect on the exploitation of the groundwater in the study area (Youssef and Ezz El-Din) [6].

The existing surface water canals in El-Bustan area are mainly excavated through the Quaternary deposits and, consequently, a direct connection between the surface water and the Quaternary aquifer is expected. Regionally, the main existed canals which considered as the main resource of the surface water are: -El-Rayah El-Naseri (about 21.8km length), El-Nubariya Canal (about 50.3km length) and El-Nasr Canal (about 22.6km length). Beside these main canals, the old El-Bustan Canal is branched from El-Nasr Canal and El-Bustan Extension Canal is branched from El-Nubariya Canal. According to El Tablawi [7]., the surface water has the following three flow directions:

- The first one is from El-Rayah El-Naseri to El- Nubariya Canal, then to the old El-Bustan canal then to El-Bustan Extension Canal.
- The second one is from El- Nubariya Canal to El-Nasr Canal.

The third one is from El-Nasr Canal to the old El-Bustan Canal and then to the secondary canals branched from the last**.**

METHODOLOGY AND INTERPRETATION TECHNIQUES

Through the present work, an integrated geoelectrical and hydrological measurements were conducted to achieve the objectives of this study.

3.1. Vertical Electrical Soundings (VES)

Time-lapse Vertical Electrical Sounding (VES) measurements were carried out using Schlumberger electrodes configuration at seventeen locations (Fig. 4) in 1992 (DRC) [8]. and 2011. The distance between the two current electrodes was varied between 2m and 1000m. As a means of control on interpretation of the VES data; three VES (6, 10, and 14) were carried out beside drilled wells (25, 18 and 11), respectively in order to tie results of the VES interpretation to hydrogeological inferences of the wells. The apparent resistivity curve was then plotted for each VES point and qualitatively interpreted to obtain preliminary information about the subsurface geoelectrical succession and their layering parameters in terms of resistivity and thickness for the two dates (1992 and 2011). Quantitative interpretation was then carried out using the layering parameters obtained from qualitative interpretation as initial layering models in computerized

interpretation software Resist [9] and RESIX-PLUS V.2.39 [10]. with hydrogeological data from drilled well as a control.

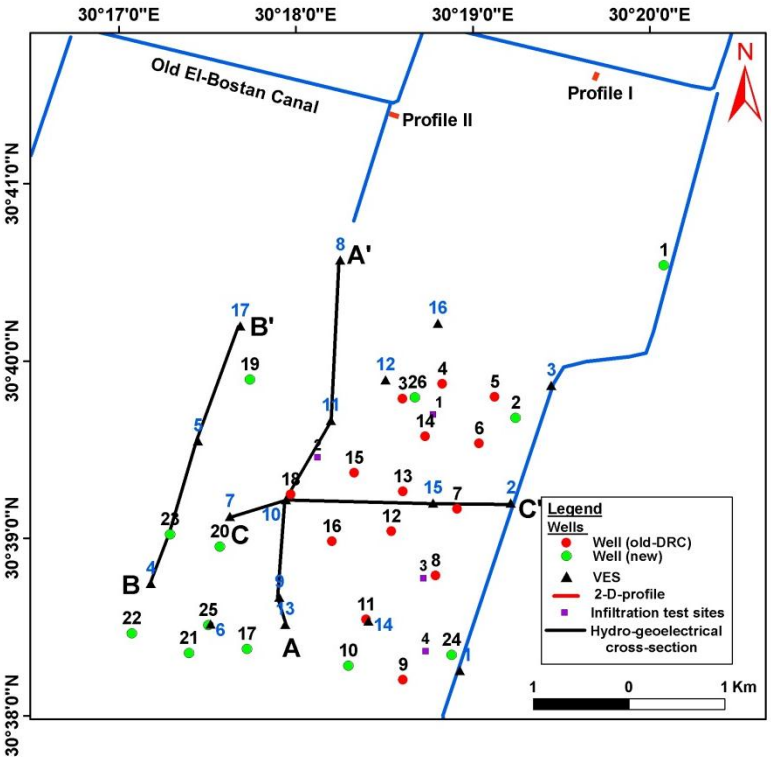

Fig. 4: Location map of the drilled wells, infiltration test, VES, hydro-geoelectrical cross sections and the two dimensional Electrical Resistivity Tomography profiles

3. 2. Two Dimension (2-D) Electrical Resistivity Tomography (ERT)

2-D ERT technique of Dipole-Dipole array was measured along two profiles perpendicular to El Bustan canal. The two profiles were carried out perpendicular to the observed cracks in El Bustan canal (Fig.4). The aim of these measurements is to detect if there is a leakage of surface water from the canal or not. Each profile has a length of 90 m, where the first electrode locates at the beginning of the profile (0m) and the last electrode No.31 is at the end of the profile (90m distance). The distance "a" between the current electrodes is the same as that between the potential electrodes (a=3m). The distance between the electrodes and the potential electrode is the dipole separation factor and is usually an integer multiple, n, of the distance between the current or potential electrode pair. Therefore, the dipole separation factor "na" was increased successively from 3 meter to a maximum value of 21meter (i.e. 3, 6, .,

21 m.) to avoid the noisy data for more the integer multiple "n". The first profile was in NE-SW azimuth while the second profile was along NNW-SSE azimuth. A forward modeling subroutine employing non-linear least square optimization technique (De Groot-Hedlin and Constable) [11]; (Loke and Barker) [12]. was then used to obtain 2-dimensional subsurface resistivity model which was subsequently subjected to iteration and inverted using RES2DINV (Loke) [13].

The Terrameter SAS 300 and Terrameter SAS 1000 resistivity meters were used during this survey for measuring the resistance "R" for each electrode separation with high accuracy.

3.3. Hydrological measurements

In the present work, hydrological field data of DRC [8]. and the present measurements in 2011 were undertaken through the investigation of 26 wells tapping the Pleistocene aquifer. Also, four pervious infiltration tests (Ismail) [14]. were used to assess the infiltration rate of the soil and its impact on the water logging in the study area.

3.4. Hydrochemical analysis of the Pleistocene Aquifer:

Twenty three groundwater samples were collected from the different locations at the study area in 2011. Chemical analyses of major ions (Ca^{2+}, Mg^{2+}, Na^{+}, K^{+}, HCO_3^{-}, CO_3^{2-}, SO_4^{2-} and Cl^{-}) were carried out at the laboratory of the Desert Research Center to compare the quality (salinity) of the groundwater with that measured in 1992.

3.5. Construction of thematic maps

The thematic maps of the area were constructed using geometrically corrected two landsat images acquired in 2002 and 2009 to reveal the development in agricultural activities and its relation to rise in groundwater level.

RESULTS AND DISCUSSIONS

4.1. Vertical Electrical Soundings

The qualitative interpretation shows that some of the field apparent resistivity curves obtained from interpretation of VES data acquired in 1992 (DRC, 1992) and after time lapse in 2011 are shown in Figure 5. The field resistivity curves in the study area are variable, where some curves that were measured in 1992 have HAK-type ($\rho_1>\rho_2<\rho_3<\rho_4>\rho_5$) but after time lapse they have HKHK type

($\rho_1>\rho_2<\rho_3>\rho_4<\rho_5>\rho_6$) in 2011 as VES 4. On the other hand, some curves have QQ–type curve ($\rho_1>\rho_2>\rho_3>\rho_4$) or Q-type ($\rho_1>\rho_2>\rho_3$) either were measured in 1992 or after time lapse in 2011 as VES 5 and 7 respectively. The difference in the resistivity values between the measured curves in 1992 and that measured in 2011 are mainly attributed to the difference of the layers boundaries, saturated zone and groundwater salinity.

The quantitative interpretation of the resistivity sounding measurements and the hydrolgeological data of the drilled wells led to the detection of three main geoelectrical units A, B, and C (Table 1). To clarify the vertical and horizontal distribution of the sedimentary succession through the two dates (1992 and 2011), three hydro-geoelectrical cross sections (Figs. 6, 7 and 8) were carried out along the area of study. A description of each of these units is given as follows :

Unit A

This unit consists of a group of thin layers differ in numbers from one VES to another. The calculated average transverse resistivity values of this unit varied from 97 Ohm.m at VES 8 to 380 Ohm.m at VES 1 in 1992 whereas, these resistivity values ranged from 75 Ohm.m at VES 6 to 395 Ohm.m at VES 16 in 2011(Fig. 9A). These resistivity values corresponds to a group of thin layers of dry clayey sand, sand and gravels, sandy clay and clay lenses. The clay lenses generally, had resistivity values less than 16 Ohm.m. The total thickness of unit "A" varied from 9 m at VES 17 to 26 m at VES 15 in 1992. On the other hand, the total thickness of the same unit varied from 3 m at VES 17 to 21 m at VES 15 in 2011 (Fig. 9B). The thickness of unit "A" represents the depth to water in the study area.

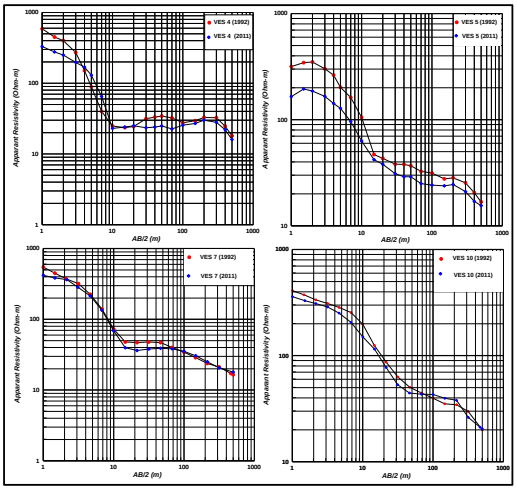

Fig. 5: Examples of the measured field curves in El Bustan area

Unit B

The geoelectrical unit "B" represents the saturated zone in the study area. Based on the exhibited geoelectrical resistivities, this unit can be differentiated into two parts. The upper part (geoelectrical layer B1) consists of clayey sand and sand. It has an average transverse resistivity values varied from 18 Ohm.m at VES 16 to 64 Ohm.m at VES 1 in 1992, whereas, in 2011 these resistivity values varied from 20 Ohm.m at VES 16 to 67 Ohm.m at VES 1(Fig. 9C). The thickness of layer "B1" has a range of of 30 - 40 m in 1992 , while this range decreases to be 36 - 49 m in 2011 (Fig. 9D). The increase in thickness of this layer in 2011 is attributed to the rise of the water table. The lower part (geoelectrical layer B2) has higher resistivity values than that of the overlying layer "B1". Its resistivity values have a range of 26 - 109 Ohm.m in 1992, whereas, these resistivity values have a range of 24 - 102 Ohm.m in 2011 (Fig.7E). These resistivity values correspond to deposits vary from clayey sand, gravely sand to gravel. The thickness of layer "B2" ranges between 32 m at VES 13 and 40 m at VES 8 in 1992 as well as in 2011.

Unit "C"

The last detected geoelectrical unit "C" exhibits relatively low resistivity values comparable with the other two units. It has resistivity values varying from 9 Ohm.m at VES 4 to 26 Ohm.m at VES 1 in 1992,

whereas, these resistivity values ranged between 7 Ohm.m at VES 4 and 23 Ohm.m at VES 1 in 2011. These resistivity values correspond to clay and sandy clay deposits.

Table (1): layering parameters for the VES stations measured in 1992 and after time lapse in 2011

VES No.	Units	layers	1992			2011			Differences in thickness (2011-1992)
			Resistivity Ω. m	Thickness (m)	curve type	Resistivity Ω. m	Thickness (m)	curve type	
1	A	A	390	18	QQ	494	14	QQ	-4
	B	B1	64	37		67	41		4
		B2	36	36		33	36		0
	C	C	26	……		23	……		
2	A	A	136	17	HK	126	13	QHK	-4
	B	B1	62	38		57	42		4
		B2	39	37		43	37		0
	C	C	18.5	……		17	……		
3	A	A	146	16	QQ	136	12	QQ	-4
	B	B1	39	40		41	44		4
		B2	34	36		37	36		0
	C	C	20	……		19	……		
4	A	A	109	15	HAK	161	12	HKHK	-3
	B	B1	40	35		39	38		3
		B2	109	37		102	37		0
	C	C	9	……		7.3	……		
5	A	A	123	17	HK	100	7	HKHK	-10
	B	B1	19	34		22	44		10
		B2	79	36		58	36		0
	C	C	14	……		13	……		
6	A	A	116	16	Q	75	4	QQ	-12
	B	B1	51	39		55	51		12
		B2	60	34		54	34		0
	C	C	14	……		12	……		
7	A	A	112	15	Q	246	5	QQ	-10
	B	B1	39	34		50	44		10
		B2	26	39		24	39		0
	C	C	16	……		15	……		
8	A	A	97	14	QQ	88	4	QQ	-10
	B	B1	34	33		31	43		10
		B2	40	40		39	40		0
	C	C	18	……		17	……		
9	A	A	205	14	QQ	168	5	HKQ	-9
	B	B1	52	38		52	47		9
		B2	106	34		96	34		0
	C	C	15	……		14	……		
10	A	A	122	23	HK	154	13	HK	-10
	B	B1	46	34		39	44		10
		B2	55	37		52	37		0
	C	C	19	……		18	……		
11	A	A	189	17	HK	165	3	QHK	-14
	B	B1	25	33		26	47		14
		B2	62	38		64	38		0

	C	C	15	……		15	……		
12	A	A	131	21		126	11		-10
	B	B1	20	36		24	46		10
		B2	26	37	HK	26	37	QQ	
	C	C	16	……		15	……		
13	A	A	128	21		90	11		-10
	B	B1	42	35	HK	55	45	QQ	10
		B2	63	32		71	32		0
	C	C	16	……		16	……		
14	A	A	119	22		152	17		-5
	B	B1	28	31	HK	29	36		5
		B2	60	37		62	37	HAK	0
	C	C	15	……		15	……		
15	A	A	142	26		139	21		-5
	B	B1	57	34		53	39		5
		B2	57	38	HK	44	38	QHK	0
	C	C	12	……		12	……		
16	A	A	145	23		151	17	QHK	-6
	B	B1	18	33	QQ	20	39		6
		B2	27	35		24	35		0
	C	C	18	……		17	……		
17	A	A	101	9		115	3		-6
	B	B1	27	37		34	37		0
		B2	63	37	HK	59	37	HK	0
	C	C	16	……		15	……		

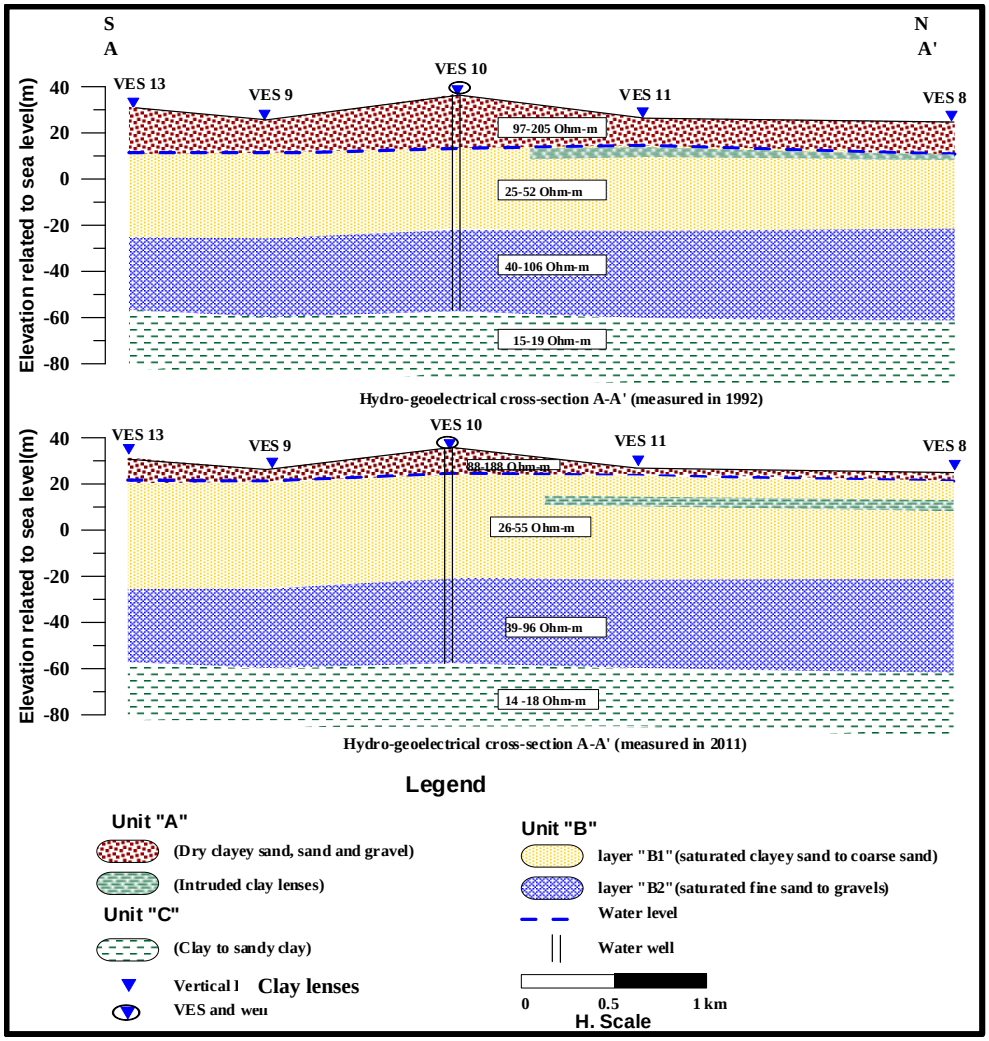

Fig. 6: Hydro-geoelectrical cross section A-A' measured in 1992 and 2011

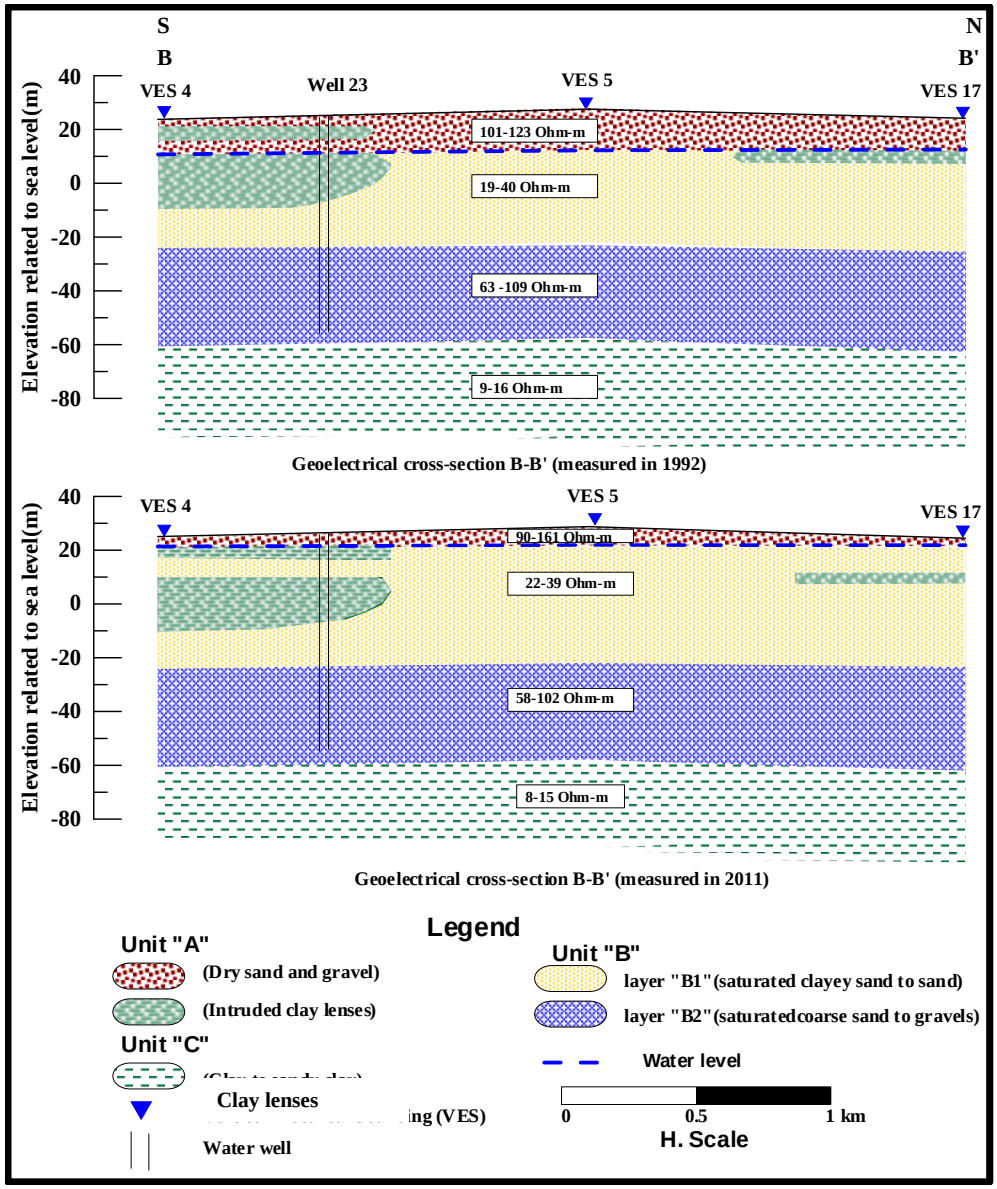

Fig. 7: Hydro-geoelectrical cross section B-B' measured in 1992 and 2011

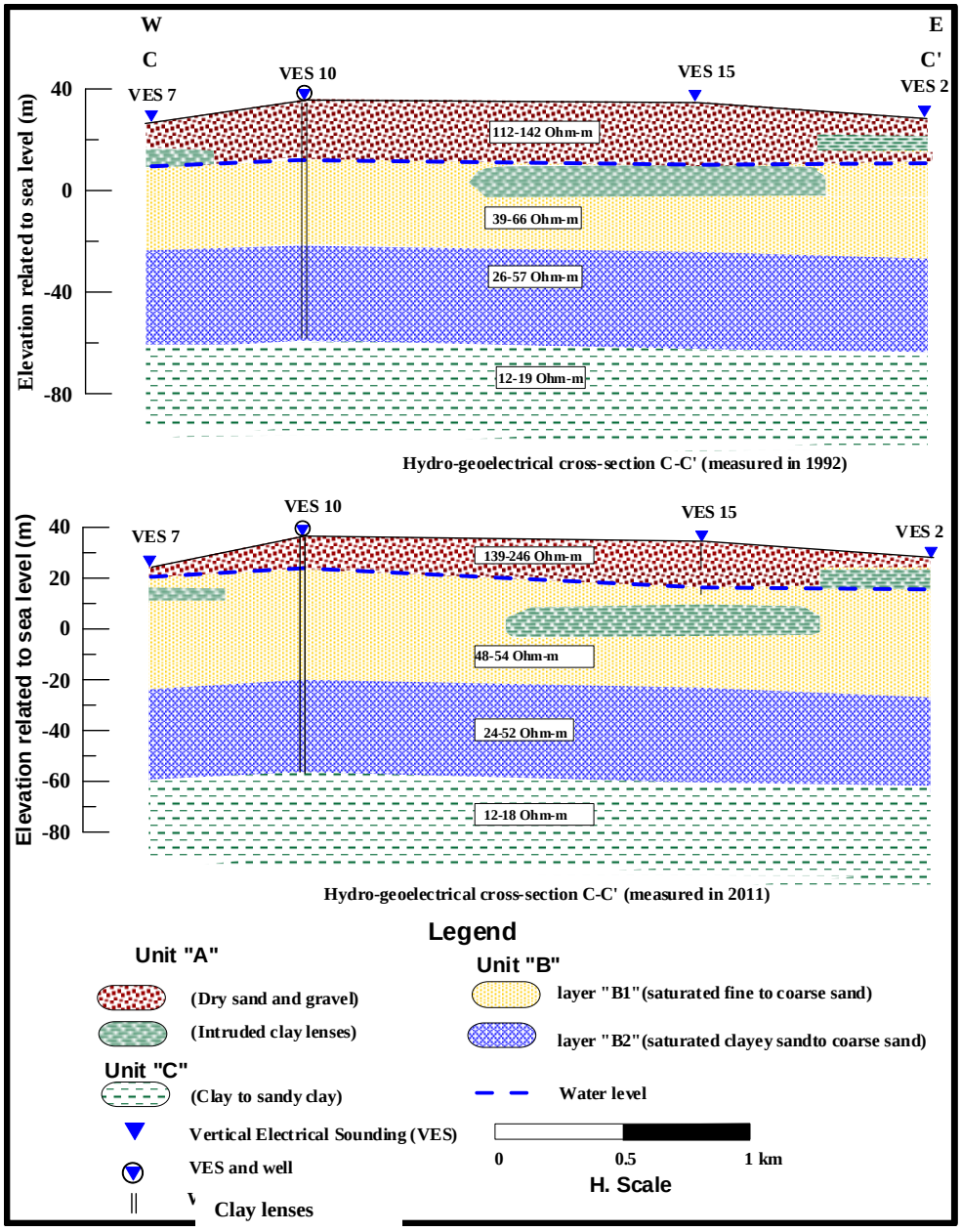

Fig. 8: Hydro-geoelectrical cross section C-C' measured in 1992 and 2011

From the constructed hydro-geoelectrical cross-sections the following common features can be deduced:

1- The base of unit "A" and / or the top of unit "B" is dominated by clay lenses at some sounding stations in the constructed hydro-geoelectrical cross-sections in 1992. Sometimes these lenses are continuous for a long distance between the measured stations. These lenses underneath or overlie the water table, thereby these lenses contribute in rising the water table at the long run of time via preventing the downward percolation of irrigation water. The clay lenses have resistivity values ranging from 3 to 15 Ohm.m.

2- After time lapse, the previous discussed lenses became an incorporated part of the geoelectrical layer "B1 in the constructed hydro-geoelectrical cross-sections in 2011," due to the continuous rise of water table.

3- The resistivity values of the dry zone (unit “A”) and the upper part of the saturated zone (layer B1) that measured after time lapse in 2011 sometimes have more or less resistivity value than that measured in 1992. The increase in the average transverse resistivity value of geoelectrical layer "B1 may due to the newly saturated part that added to geoelectrical layer "B1" was consisting of coarse sand and gravel, this rises the transverse resistivity value of layer "B1" and in the same time may decrease the transverse resistivity value of unit "A”.

4- Also, the direct water seepage from Canals may decrease the salinity of saturated water of geoelectrical layer “B1”. So, its resistivity value increases. Inversely, The decrease in the average transverse resistivity value of geoelectrical layer "B1 may be due to the newly saturated part that added to geoelectrical layer "B1" was consisting of fine sand and clay, this decreases the transverse resistivity value of layer "B1" and may increase the transverse resistivity value of unit "A” also. Another factor controls the decrease in resistivity value is represented by the seepage from irrigation water that increase the salinity of groundwater.

4.2. Two-Dimensional Electrical Resistivity Tomography (ERT):

The true resistivity plot of the 2-D imaging profile at the first site (Fig. 10) revealed that this model consists of three zones. The first zone consists of dry coarse deposits of sand and gravels having resistivity values ranging from 115 to more than 185 Ohm.m. The

thickness of this zone varies from 2 m in the Northeastern end of the profile, about 5 m in the middle distance (beneath electrode 42 m) and 4 m in the southwestern end of the profile (beneath the electrode value 6 m). The second zone consists of fine deposits and is represented the wetted zone above water table due to the vertical percolations of the irrigated water or the lateral seepage from the canal. This layer is underlain by clay lenses which having the lowest resistivity values at some places along the profile. The vertical percolation of irrigation water and the lateral seepage from surface canals making the continuous rising up of the water above the impervious clay lenses causing the problem of water logging. The fine deposits extends to depth of 5 m. These deposits have resistivity values ranging from 13 to 92 Ohm.m. The third zone represents the water-bearing zone starting from depth 5 m and extends to the end of the section. Generally, the saturated zone has a lateral variation in resistivity values that varies from 8 to 43 Ohm.m. as illustrated by arrows on the inverted resistivity section. Hence most of the northeastern part (beneath electrode values 90m to 72m) has a lower resistivity values comparable with the other parts of the section either over or under the water table. This could be attributed to the seepage from El Bustan canal.

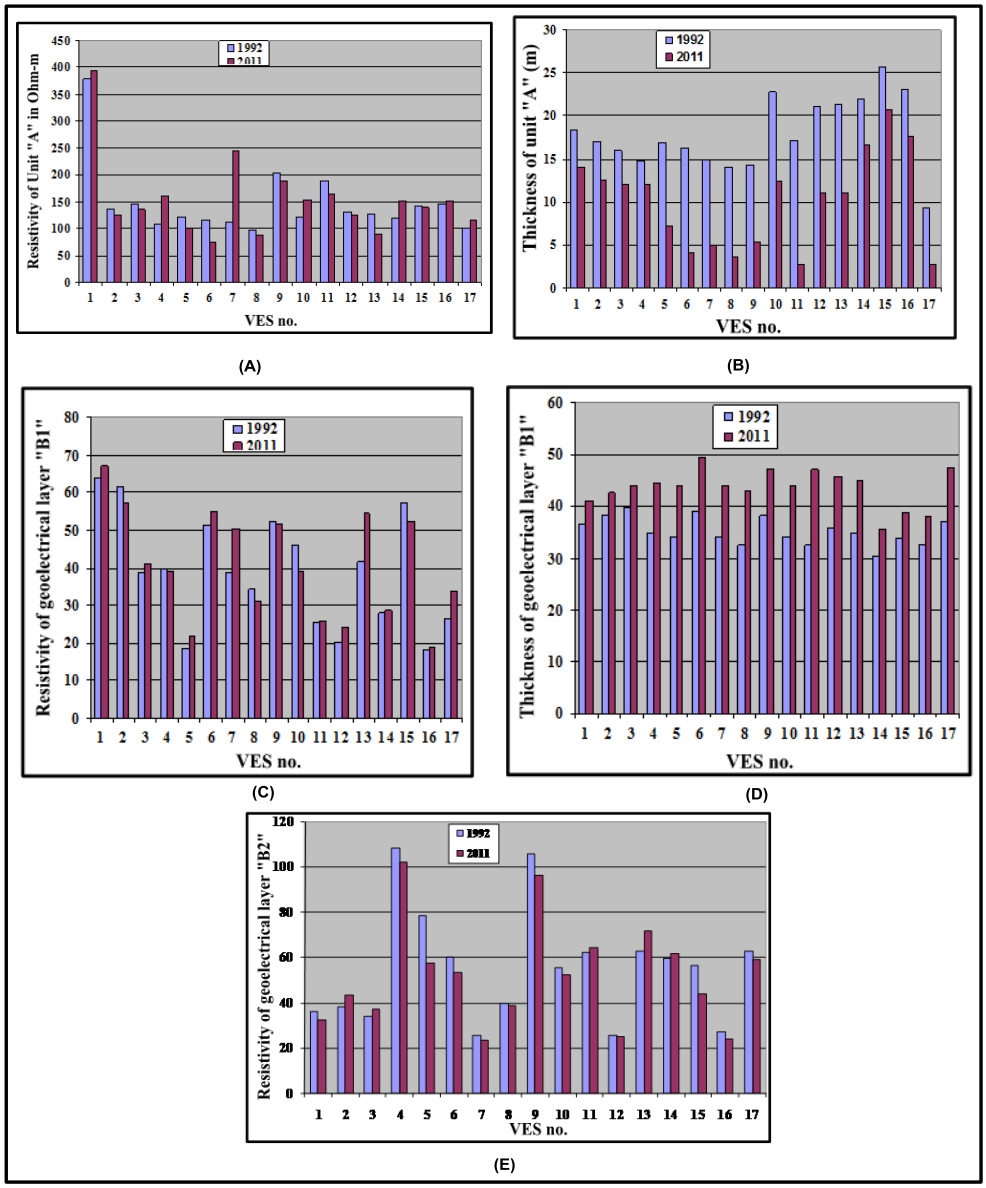

Fig. 9: Bar diagrams demonstrate the variation of:

(A): the transverse resistivity of layer A, (B): The thickness of layer A,

(C): the transverse resistivity of layer B1, (D): The thickness of layer "B1" and

(E): the resistivity of layer "B2" with time

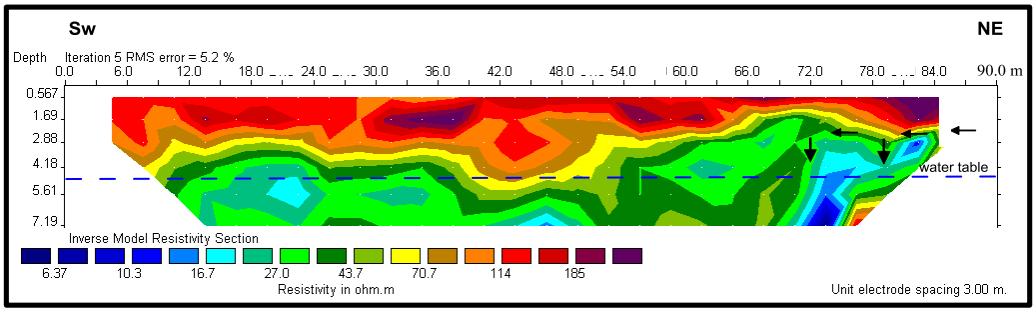

Fig. 10: Inverted resistivity model of 2-D imaging profile at the first site

The true resistivity plot of the 2-D imaging profile at the second site (Fig. 11), revealed that this model consists of dry zone have resistivity values ranging from 79 to more than 238 Ohm.m suggesting deposits of sand and gravels. The dry zone extends up to a depth of 5.5 m. The saturated zone follows the dry zone and has resistivity values ranging from 26 to 126 Ohm.m corresponding to clayey sand to sand deposits. In the side facing El Bustan Canal at the WNW part of the section, beneath the electrode location of 81 m and 84 m surface water could seep from the Canal through sand as illustrated by the arrows through the inverted resistivity section at the WNW end of the profile in Figure 11.

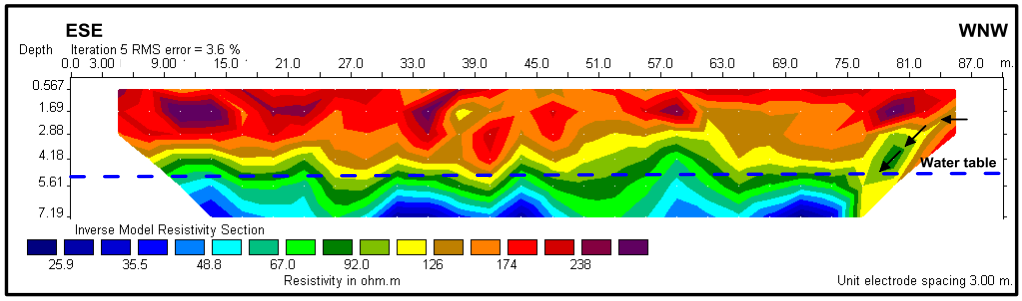

Fig. 11: Inverted resistivity model of 2-D imaging profile at the second site

4.3. Depth to water and water level of the Pleistocene Aquifer

The total drilled depths of the investigated wells range between 84 m and 150 m. The groundwater of the Pleistocene aquifer in the study area was encountered in 1992 at depths ranging between 9 m at the northwestern part (VES No. 17) and 28 m at the eastern part (Well No. 5), while in 2011, it existed at depths varying from 2 m (VES No. 17) to 23m (Well No. 2) (Fig. 12). This reflected an increase in water level between 1992 and 2011. This is as corroborated by depth to water contour map

and water level map constructed for the two different periods (1992 and 2011) shown in Figure 12 and 13, respectively.

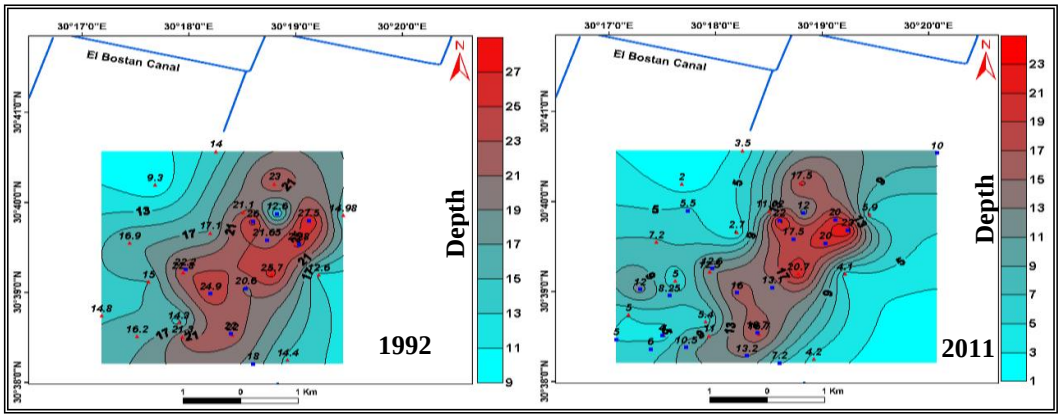

Fig. 12: Depth to water maps in years 1992 and 2011

Fig. 13: Water level maps in year 1992 and 2011

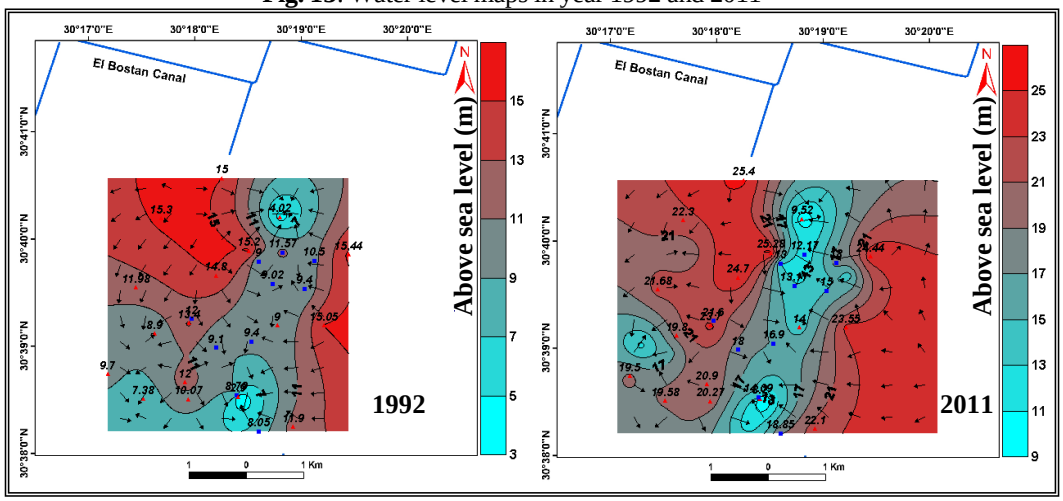

These maps show that the water level values range between 3-15 m and 8-25 m above mean sea level in 1992 and 2011, respectively with some local changes in the flow direction.

The resultant groundwater level contour map taking into consideration the different in water level in 1992 and 2011 at all localities in the study area is as depicted in Figure 12. This map shows that there is an increase in the groundwater levels all over the area with different values. The maximum rising in the groundwater level is 14 m at the western part of the study area, while the minimum rising is less

than 1 meter at the northeastern part. This could be attributed to percolation of infiltrated water from irrigation and precipitation. Thus the continuous rising of the water levels and the lack of adequate drainage system will subject the cultivated areas to be water-logged.

There is a direct relation between the maximum rates at which the excess irrigation water can enter a particular soil which known as the infiltration capacity and the rising of the water table. The data of four previous infiltration tests (Ismail, 1994)[14] in the study area were used to determine the contribution of soil structure on the water logging. The infiltration test sites were plotted with its values on the resultant water level contour map of the study area between 2011 and 1992 as shown on Figure 14. The values of the infiltration rate ranges between 25 – 372 mm/h as shown in Table (2) and also the soil structure assessment according to (Geeves et al.) [15].. It is noticed that the location of the lowest value of infiltration rate (25 mm/h) in the northeastern part of the study area has the lowest value of rising water table and vice versa for the location of highest value of infiltration rate (372 mm/h) has the highest value of rising water table at the western part.

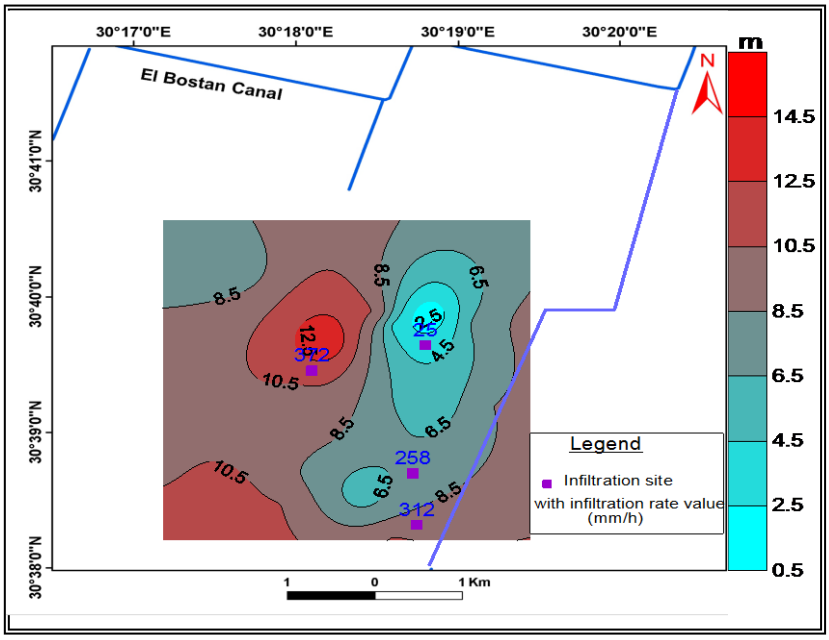

Fig. 14: Resultant water level contour map of the study area

Table (2): The infiltration tests data and soil structure assessment (according to Geeves et al.) [15]

Test No.	Infiltration rate (mm/h)	Soil structure assessment depending on infiltration ra value according to Geeves et al., 1995
1	25	Poor structure quality (infiltration rate 10 - 30 mm/h
2	372	Good structure quality (infiltration rate > 70 mm/h)
3	258	Good structure quality (infiltration rate > 70 mm/h)
4	312	Good structure quality (infiltration rate > 70 mm/h)

The wide range of rate of water entry (25 - 372 mm/h) is an indication that different soil types existed in the study area as shown from the direct relation between the infiltration rate and the resultant water level (Fig. 15) which indicates that the infiltration site number one which has low values of both infiltration rate and resultant water level can be classified according to (Geeves et al., 1995) [15]. As poor structure quality soil while the other three sites can be classified as good structure quality.

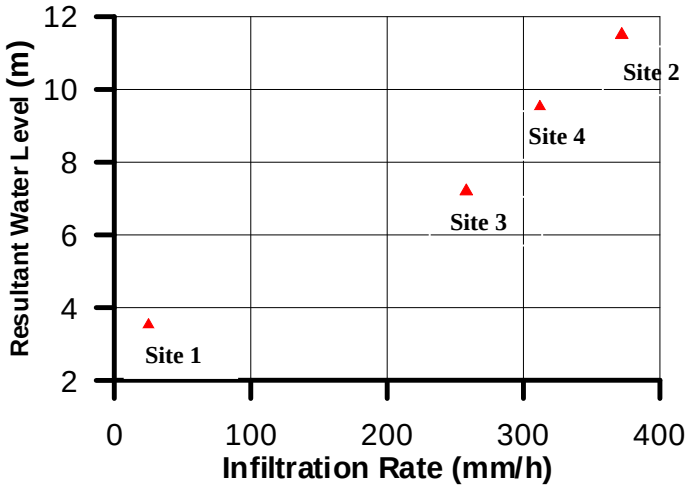

Fig. 15: The relation between the infiltration rate and the water level resultant

4.4. Hydrochemical Characteristics of the Pleistocene Aquifer

The analyzed major cations and anions data of the groundwater samples and El-Bustan canal sample (Table 3) are plotted on the Piper [16]. Trilinear diagram (Fig. 16). The diamond field of Piper diagram can be subdivided into 4 main Sub-Fields, each of them has its own characteristics, as follows:

- Sub-Field No. I; is characterized by $NaHCO_3$ + Ca – Mg $(HCO_3)_2$.
- Sub-Field No. II; is characterized by Na_2SO_4 + $NaHCO_3$ water.

- Sub-Field No. III; is characterized by NaCl + Ca – MgCl.
- Sub-Field No. IV; is characterized by Ca – $MgSO_4$ + Ca – $MgCl_2$.

The plotted chemical data on Piper's diagram shows the following:

1- In the cation triangle, all the groundwater samples are of high percent sodium, i.e. sodium ions are predominating.
2- In the anion triangle, the samples are distributed between Cl^- and $HCO3^- + CO_3^{2-}$.
3- The groundwater is actually high in sodium and potassium and differ in the anion content, 39 % of the samples falls in the sub-field No. II which characterized by NaHCO3 water type where the source of recharge of the Pleistocene aquifer mainly from the Nile water while, 61 % of the samples falls in the sub-field No. III having NaCl water type on the diamond field indicating that the study area is affected by the leaching process of excess irrigation water that increase the salinity of the groundwater.

The iso-salinity contour maps were constructed for the two different dates (Fig. 17) which reveal that the groundwater salinity values range between 662-1715 ppm and 486-1509 ppm in 1992 and 2011, respectively.

Table (3): Chemical analysis results for the groundwater samples and El-Bustan Canal sample in 2011.

Well	TDS	Ca^{++}		Mg^{++}		Na^+		K^+		HCO_3^-		CO_3^{--}		SO_4^{--}		Cl^-	
No.	Ppm	ppm	epm	ppm	epm	ppm	epm	ppm	Epm	ppm	epm	ppm	epm	ppm	epm	ppm	epm
1	505	3.1	0.1	3.10	0.2	155	6.7	7.0	0.2	220	3.6	42.0	1.4	12.0	0.3	61.9	1.8
2	741	13.3	0.7	14.3	1.2	230	10	9.0	0.2	140.5	2.3	30.0	1.0	5.0	0.1	295.1	8.4
4	1033	20.4	1	21.1	1.7	335	14.6	8.5	0.2	122.2	2.0	12.0	0.4	17.0	0.4	490.3	14.0
5	1509	4.1	0.2	3.7	0.3	510	22.2	19.5	0.5	403.3	6.6	78.0	2.6	10.0	0.2	471.2	13.5
6	585	6.1	0.3	7.4	0.6	180	7.8	6.0	0.2	207.7	3.4	36.0	1.2	4.0	0.1	135.7	3.9
8	704	16.4	0.8	11.2	0.9	215	9.4	7.0	0.2	189.4	3.1	48.0	1.6	5.0	0.1	209.4	6.0
9	992	3.1	0.2	4.3	0.4	340	14.8	14.0	0.4	244.4	4.0	48.0	1.6	10.0	0.2	323.7	9.3
10	511	6.1	0.3	5.6	0.5	150	6.5	3.5	0.1	220.0	3.6	42.0	1.4	6.0	0.1	76.2	2.2
11	699	6.1	0.3	6.8	0. 6	230	10.0	4.0	0.1	201.6	3.3	48.0	1.6	10.0	0.2	189.0	5.4
12	843	2	0.1	3.1	0.3	275	12.0	9.0	0.2	317.7	5.2	48.0	1.6	10.0	0.2	175.0	5.0
13	551	4.1	0.2	6.2	0.6	173	7.5	4.0	0.1	207.7	3.4	48.0	1.6	4.0	0.1	102.3	2.9
14	902	1	0.1	3.1	0.3	300	13.0	15.0	0.4	262.7	4.3	60.0	2.0	10.0	0.2	242.8	6.9
16	1097	14.3	0.7	3.7	0.3	370	16.1	15.0	0.4	244.4	4.0	30.0	1.0	20.0	0.4	395.1	11.3
17	514	13.3	0.7	5.5	0.5	155	6.7	4.5	0.1	171.1	2.8	36.0	1.2	5.0	0.1	122.5	3.5
18	1183	3.1	0.2	1. 9	0.2	400	17.4	13.0	0.3	299.4	4.9	54.0	1.8	25.0	0.5	380.8	10.9
19	736	7.2	0.4	9.9	0.8	230	10.0	8.5	0.2	201.6	3.3	36.0	1.2	15.0	0.3	223.7	6.4
20	1149	10.2	0.5	13.0	1.1	397	17.3	8.5	0.2	177.2	2.9	36.0	1.2	30.0	0.6	471.2	13.5
21	837	20.4	1.0	16.1	1.3	230	10.0	7.0	0.2	201.6	3.3	18.0	0.6	25.0	0.5	315.0	9.0
22	1127	14.3	0.7	13.6	1.1	380	16.5	7.0	0.2	152.8	2.5	30.0	1.0	30.0	0.6	493.6	14.1
23	612	4.1	0.2	8.1	0.7	184	8.0	4.5	0.1	244.4	4.0	30.0	1.0	6.0	0.1	128.5	3.6

24	486	9.2	0.5	5.6	0.5	145	6.30	7.5	0.2	158.9	2.6	30.0	1.0	23.3	0.5	105.0	3.0
25	947	16.4	0.8	18.0	1.5	300	13.0	7.5	0.2	134.4	2.2	18.0	0.6	33.3	0.7	414.1	11.8
26	574	8.2	0.4	6.8	0.6	167	7.3	4.0	0.1	256.6	4.2	30.0	1.0	3.33	0.1	97.3	2.8
27	290	18.4	0.9	7.4	0.6	46	2.0	7.0	0.2	146.6	2.4	18.0	0.6	10.0	0.2	35.7	1.0
	sample no. 27 is equivalent to El Bustan Canal																

The difference between Iso-salinity contour maps of the years 1992 and 2011 are used to construct the resultant groundwater salinity contour map (Fig. 17). It indicates that the resultant salinity ranged from -1200 ppm through 300 ppm. The zero salinity value contour line indicates that there is no change in the groundwater quality between the two dates, the negative salinity values means that there is a decrease in the groundwater salinity in the eastern part of the study area which may be attributed to the seepage and interflow from the eastern branch of El-Bustan canal since the salinity of its water is 290 ppm. The positive salinity values indicate that there is an increase in the groundwater salinity in the western part of the study area which may be attributed to the excess irrigation water that percolates after leaching the soil and is stored underground changing the original hydrochemistry of the local aquifer, consequently increasing the water salinity.

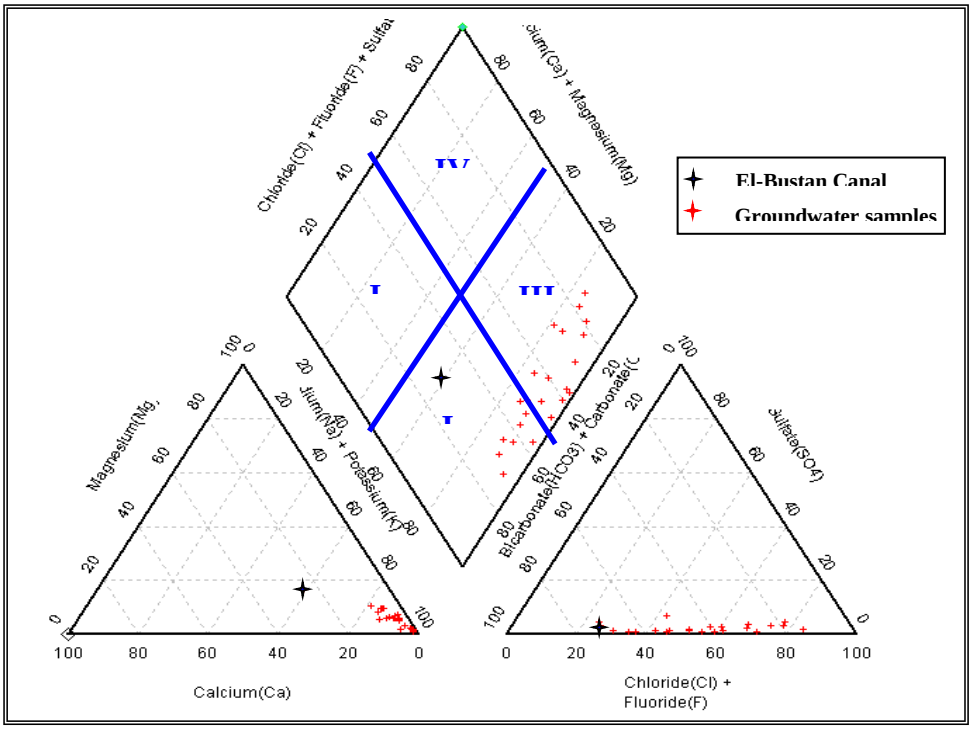

Fig. 16: Piper Trilinear diagram for hydrochemical classification of the groundwater samples in the study are

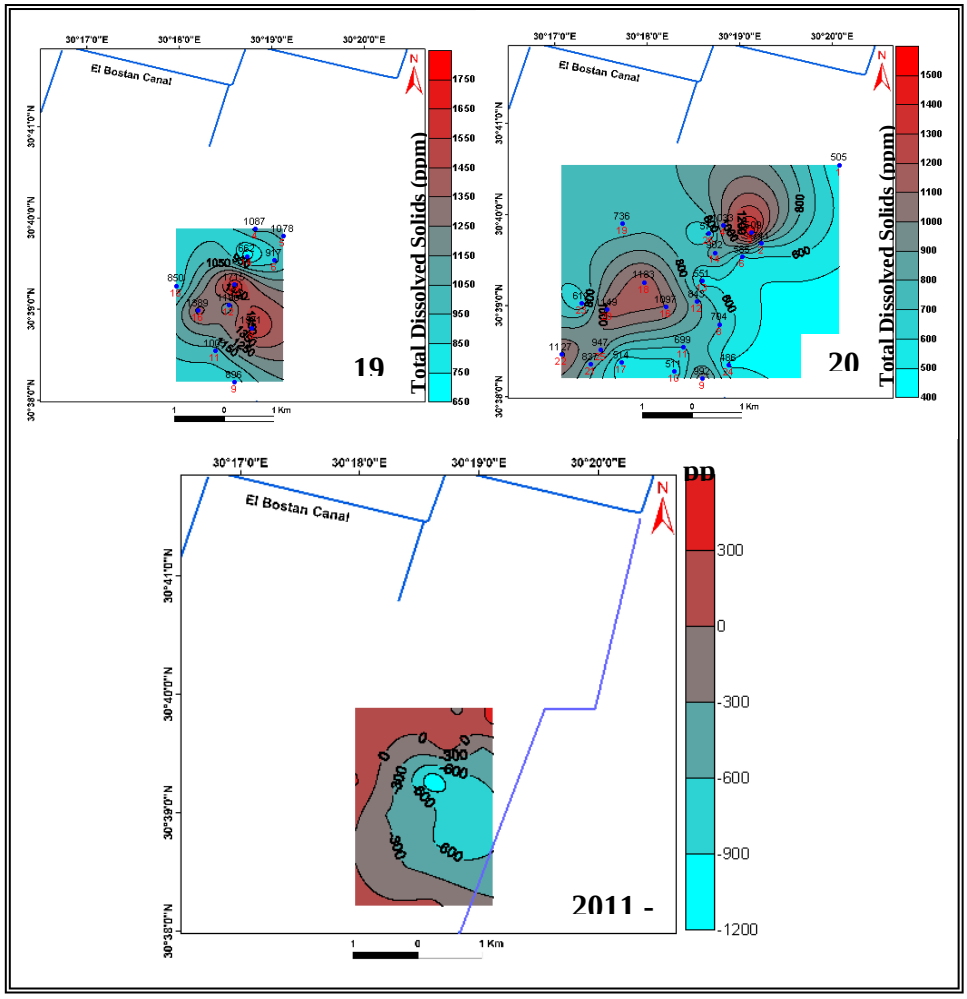

Fig. 17: Iso- salinity maps for the groundwater in years 1992 and 2011 and the Resultant groundwater salinity map (2011-1992) (Contour values in ppm)

4.5. The contribution of the topography on the water logging in the study area

Topography is considered as one of the natural causes that has an important bearing on the drainage of the study area. The topography of the study area is shown through the digital elevation model (DEM) (Fig. 18) which shows that the areas with elevation less than 15 m above mean sea level are very limited, the majority of the study area has elevation range between 15-30 m above mean sea level and there are

scattered elevated areas with range 30-54 m above mean sea level. The water level resultant contour lines between the two different dates 2011 and 1992 are plotted on the DEM map to detect the contribution of the topography on the water table rising. From Figure 18, it is clear that the western side of the study area are more affected by the water table rising since the existing of flat lowlands tend to become waterlogged naturally because the excess irrigation water flows on the surface and concentrates in these lowlands having enough time to infiltrate and

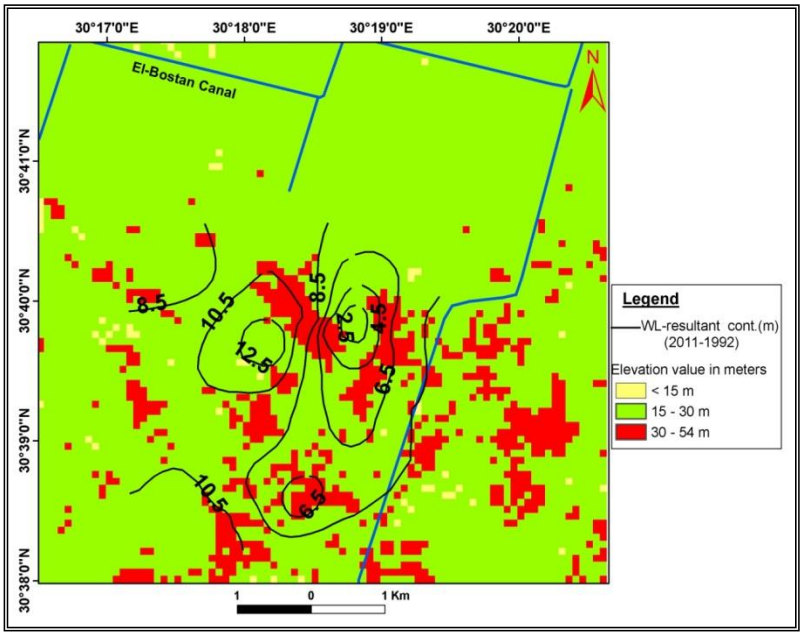

percolate down raising the water table especially this area has high values of the infiltration rate (372.08 mm/h) with good structure quality soil as discussed before.

Fig. 18: The digital elevation model (DEM) of the study area and the water level resultant contours

4.6. Agricultural development in the study area

Two different satellite images data (2002 and 2009) were visually interpreted to quantify the surface data for the assessment and measurement of the development activities. From the visual interpretation of the Landsat ETM 2002 and 2009 for the study area, thematic maps (Fig. 19) have been constructed showing that the cultivated area is 2456 Hectar in 2002 while for the date 2009; the cultivated area is 3647 Hectar which means that there is an increase in the cultivated area with value of about 1191 Hectar. The study area

subjected to faulty irrigation practices such as flood irrigation system and cultivation of high water requirements crop such as banana which are considered from the human-induced causes contributing to the problem of water logging.

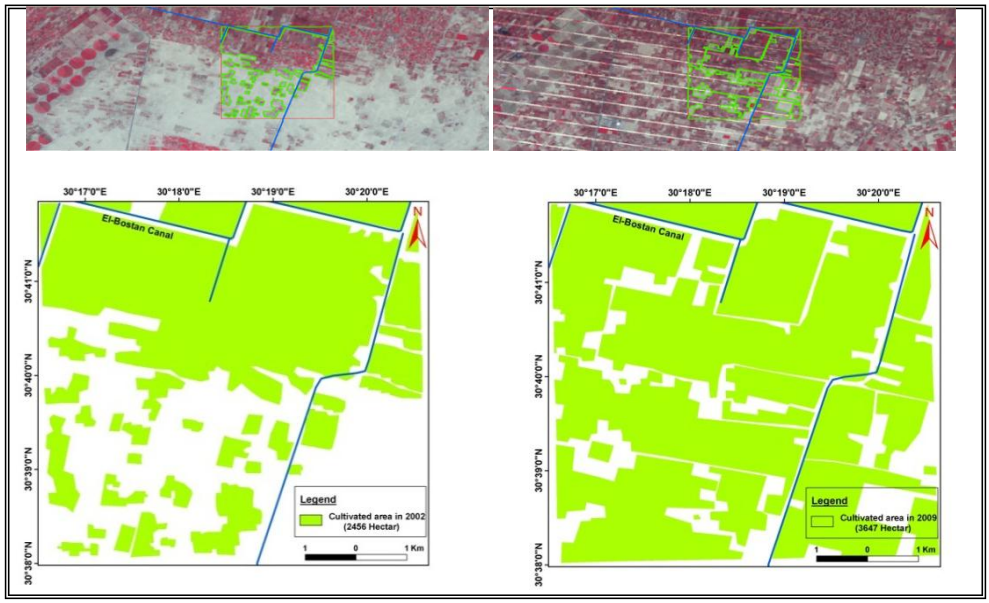

Fig. 19: Thematic maps showing the cultivated land in the study area interpreted from landsat data (2002 and 2009)

4.7. Management to control the impact of water logging

There are many factors must be considered when trying overcoming an irrigation water logging problem. Good drainage system and irrigation layout are essential to minimize the problem of water logging and increase crop production.

To ensure that the irrigation layout is well planned and designed, the development of a whole farm plan must be taken into account and also to ensure a good drainage system, the drainable surplus should be known to avoid any unacceptable rise in both groundwater and surface water levels. In general and in particular for the area under consideration, the following points may help to manage and control the negative impacts of the water logging problem:

1- Proper investigation, suitable planning and design for irrigation and drainage networks can mitigate and solve the problems of water logging to improve agricultural productivity.

2- Applying adequate drainage systems according to the natural gradient with proper maintenance from time to time to increase their carrying capacity.
3- Preventing canal seepage by lining of any damaged portions of canal network system from time to time.
4- Conjunctive use of surface and subsurface water may help in bringing down the high groundwater level especially in the sensitive areas to water logging in the northwestern part of the study area.
5- Building in a net of observation wells to monitor water levels and salinities with time.
6- Management of the drilling of new wells and water exploitation in the study area to safe the groundwater for sustainable development.
7- Applying modern irrigation systems instead of the applied flood irrigation system.
8- Stopping the cultivation of the bananas which is considered as one of the highly requirements water crops.

CONCLUSIONS

The Pleistocene aquifer is the main source of the groundwater in the study area**.** The geoelectrical and the hydrological results revealed that the water levels increase continuously with time, where it has ranges 3-15 m a.m,s.l. in 1992 and 8-25 m a.m,s.l. in 2011. The interpretation results of the 2D ERT profiles indicate the presence of seepage of surface water from El Bustan Canal. The continuous rise of water level with time in the study area has many causes. These causes include the presence of clay lenses above and beneath the water table, the seepage of surface water from Canals, applying flood irrigation system and lack of the drainage system. This rise in water level leads to water logging problem especially, in the western part of the study area. To overcome this problem a management system is recommended for the study area.

REFERENECES

[1] Shata, A. A. and El fayoumy, I. F. (1967): "Geomorphological and morphopedological aspects of the West of the Nile Delta with special reference of Wadi Natroun". Desert d'Egypt; T.XVIII. No.1, p.1-28.
[2] Shata, A. A., Pavlov, M. and Sanad, K. F. (1962): "Preliminary report on the geology, hydrogeology and groundwater hydrology of Wadi Ell

Natrun and adjacent areas", Internal report desert Institute, Cairo, Egypt, p. 159.

[3] Continental Oil Company CONOCO, (1987) Geologic map of Egypt 1:500 000 series, Sheet no. 36.

[4] Abdel Baki, A.M. (1983): "Hydrogeological and hydrogeochemical studies on the area west of Rosetta Branch and South of El Nasr Canal", "Ph.D. Thesis, Fac. Sci., Ain Shams Univ., Cairo, Egypt, 156p.

[5] Ibrahim, S. M. M. (2005): "Groundwater resources management in Wadi El-Farigh and its vicinities for sustainable agricultural development", ph.D. Faculty of Engineering, Ain Shams Univ., Cairo, Egypt, p152.

[6] Youssef, A. M. and Ezz El-Deen, H. M. (1999): "A geoelectrical study to determine the factors affecting the groundwater exploitation in El-Bustan area, west of the Nile Delta, Egypt". E.G.S. Proc. of the 17th Ann. Meet., March 1999, pp. 131-144.

[7] El Tablawi, E. E. D. (2002): "Groundwater Management for Agricultural Development in some areas West of Nubariya and South of El Nasr Canals", ph.D. Thesis, Institute of Environmental Studies and Research,. Ain Shams Univ., Cairo, Egypt, p218.

[8] Desert Research Center (1992): " Hydrogeophysical studies on El Bustan area, Western part of the Nile Delta, Egypt" Internal reports, Publications of the Desert Research Center, p87.

[9] Van Der Velpen B. P. A. (1988): "RESIST, version 1.0, a package for the processing of the resistivity soundind data", M. Sc. Research Project, ITC, Deft, the Netherlands.

[10] Interrex Limited (1996): "RESIX- PLUS. Resistivity data interpretation software", V. 2.39., Golden Colorado, USA.

[11] De Groot-Hedlin, C. and Constable, S. (1990): "Occam's inversion to generate smooth two-dimensional models from magnetotelluric data" Geophysics, 55, 1613-1624.

[12] Loke, M.H. and Barker, R. D., (1996): "Rapid least-squares inversion of apparent resistivity pseudo-sections by a quasi-Newton method". Geophysical prospecting, 44, pp. 131-152.

[13] Loke, J.(1998): " RES2DINV. V. 3.4, rapid 2-D resistivity inversion using the least-square method", ABEM instrument AB, Bromma, Sweden.

[14] Ismail, Y.L. (1994): " Hydrological studies on the groundwater reservoir in some localities under reclamation in west El-Nubaria province", MSc. Thesis, Fac. Sci., Ain Shams Univ., Cairo, Egypt.pp.127.

[15] Geeves, G., Cresswell, H., Murphy, B. and Chartres, C. (1995): " Productivity and sustainability from managing soil structure in cropping soils of southern NSW and northern Victoria on lighter textured soil surfaces", CSIRO Division of soils & NSW Dept. Land and Water Conservation.

[16] Piper, A. M. (1944): "A graphic representation in the geochemical interpretation of groundwater analyses", Am. Geophys. Union Trans., 25, 914-923.

رصد وادارة ظاهرة غدق المياه باستخدام التقنيات الجيوكهربية و الهيدرولوجية فى منطقة البستان – غرب الدلتا

***أيمن محمد محمود التهامى- *سوسن مصيلحى محمد ابراهيم**

****مركز بحوث الصحراء- المطرية- القاهرة***

تمثل الأراضى الصحراوية الواقعة غرب دلتا النيل مناطق الامتداد الطبيعى لدلتا النيل حيث بدأت مشاريع الاستصلاح الزراعى القديم بها منذ سنة ١٩٥٠ و تعتبر منطقة البستان احدى هذه المناطق التى بدأت عملية الاستصلاح بها فى العقد الأخير من القرن العشرين. استمرارارتفاع منسوب سطح المياه الجوفية سوف يسبب غدقا للمياه و تدهور للأراضى المستصلحة فى منطقة الدراسة. التكامل بين الدراسات الجيوكهربية و الهيدرولوجية سوف يساعد فى ايجاد حلول لهذه المشكلة من خلال رصد خصائص المياه الجوفية (عمق سطح المياه، مستوى سطح المياه و الملوحة) مع الوقت و اقتراح الادارة و الاستغلال الأمثل للمياه الجوفية للتغلب على مشكلة غدق المياه بمنطقة الدراسة. من خلال البيانات المتاحة من الأبار ونتائج الجسات الجهربية تم التعرف على ثلاث وحدات جيوكهربية (A, B and C) . الوحدة "A" تمثل النطاق الجاف بمنطقة الدراسة و تتكون من رمل طينى و رمال وحصى مع وجود تداخل من عدسات الطين و الطين الرملى فى بعض المواقع. سمك هذه الوحدة يمثل العمق لسطح المياه الجوفية بمنطقة الدراسة و الذى يتراوح بين ٩-٢٨ مترسنة ١٩٩٢م بينما يقل هذا السمك فى القياسات الحديثة سنة ٢٠١١ حيث تراوح هذا السمك بين ٢-٢٣ متر. الوحدة "B" تمثل التكوين الحامل للمياه الجوفية بمنطقة الدراسة و تتكون من رواسب الرمال الطينية و الرمال فى الجزء العلوى و تتغير الى رواسب الرمال الطينية و الرمل الحصوى و الحصى فى الجزء السفلى التى تتميز بمقاومة كهربية أعلى من الجزء العلوى. الوحدة الجيوكهربية "C" تمثل أخر طبقة جيوكهربية تم الوصول اليها و تتميز بمقاومة كهربية قليلة بالمقارنة بالوحدتين السابقتين نتيجة لزيادة المحتوى الطينى بها. تفسير قطاعا الجيوكهربية المقطعية اللذان تم قياسهما عموديا على ترعة البستان أوضحا وجود سريان من ترعة البستان الى الخزان الجوفى بمنطقة الدراسة. و قد أوضحت الدراسات الهيدرولوجية أن مستوى سطح المياه منسوب لسطح البحر هو 3- 15 متر سنة ١٩٩٢ و من 8-25 متر سنة ٢٠١١ و ملوحة المياه كانت ٦٦٢-١٥٧١ جزء فى المليون سنة ١٩٩٢ وانخفضت فى سنة ٢٠١١ لتصل الى ٥٠٥-١٥٠٧ جزء فى

المليون ويعكس هذا الانخفاض تسرب المياه السطحية العذبة من ترعة البستان الى الخزان الجوفى .التكامل بين الدراسات الجيوكهربية و الهيدرولوجية أدى الى تحديد أسباب مشكلة غدق المياه بمنطقة الدراسة. من خلال الرصد الدورى والادارة الجيدة للمياه الجوفية وتطوير طرق الرى سوف يؤدى ذلك الى الحد من ظاهرة غدق المياه ومن ثم الحد من تدهور الأراضى المستصلحة و زيادة انتاجيتها.